Available online at www.sciencedirect.com
ScienceDirect
Cement and Concrete Research 37 (2007) 1134–1143
Cement and Concrete Research

The corrosion resistance of coated steel dowels determined by impedance spectroscopy

David Jolivet [a], David M. Bonen [b,*], Surendra P. Shah [a]

[a] Department of Civil Engineering, Center for Advanced Cement-Based Materials, Northwestern University. Evanston, IL, USA
[b] School of Civil Engineering, Purdue University, W. Lafayette, IN, USA

Received 24 October 2005; accepted 5 April 2007

Abstract

The corrosion resistance of coated smooth steel dowels in simulated pore solution with and without 3.5% sodium chloride solution is reported. The dowels are coated with a double-layer structure composed of a 180 μm of Nickel–Chromium–Boron (referred to as NiCrB) that is overlaid by a 20 μm inorganic layer made of silicon powder, silica fume, blast furnace slag, and combinations thereof. The composition of the synthetic pore solution is based on the composition of pore fluids expressed from Type I portland cement that is characterized by pH of about 13.4 and an ionic strength of 0.4.

Alternating current impedance spectroscopy measurements conducted in the range of 10 mHz to 10 kHz were found to be instrumental in detecting any change in the resistance of the coatings. It was found that the NiCrB sub-layer provides a good corrosion resistance that outperforms that of the inorganic coating. Of the five inorganic compositions tested, the combination of slag and silica fume has the best performance. The protection against corrosion is attributed mostly to particle packing rather than densification of the matrix due to pozzolanic reaction.

Keywords: Corrosion; Steel coating; Impedance Spectroscopy; Pore solution; Pozzolanic reaction

1. Introduction

It is widely known that corrosion of reinforcing steel tops the list of concrete durability considerations [1] and the resources allocated to replace or repair premature structurally deficient bridges for example are quite substantial [2]. Rebar corrosion can be controlled by a number of measures including prevention, mitigation, and protection [3]. Prevention is related to having an adequate concrete cover over the rebar, maintaining high pH, and decreasing the permeability to keep away oxygen, water, and chloride from reaching the rebar surfaces. Oxygen and water are essential for this type of electrochemical corrosion, whereas chlorides act as an initiating agent. Chlorides break down the initial passive layer that is formed on the reinforcement surface that is further protected due to the highly alkaline environment of the cement matrix. This breakdown allows the setup of an electrolytic cell in which ferrous ions (Fe^{2+}) (cathode) are oxidized to form ferric oxide Fe_2O_3 and $(OH)^-$, anode. Then the ferric compound reacts further to give voluminous hydrous ferric oxide compounds (rust) and other Fe-oxychlorocomplexes.

At the onset, chloride induced corrosion may result in pitting that subsequently may be followed by spalling and complete mechanical disintegration of the concrete cover over the reinforcement. Effective provisions against corrosion are low permeability, a 5 cm cover or more, cement content of 400 kg/m^3, and chloride content less than 0.1% of cement by weight [4], and information related to corrosion and its mechanism is given elsewhere [5–11].

Mitigation techniques involve the incorporation of a chemical admixture such as calcium nitrite, and common protection techniques are based on coatings or cathodic protection. To date, an epoxy-based coating is the most used material. Its efficiency in protecting against corrosion is generally high provided that the coating is not damaged due to its low abrasion and impact resistance [12]. Moreover, the epoxy coating can fail without any mechanical damage because, over time, the coating may absorb moisture and disband from the steel. Once some of the coating is removed due to one of the mechanisms listed above, the internal formation of iron oxide causes debonding and cracking of the

* Corresponding author.
E-mail address: dbonen@ecn.purdue.edu (D.M. Bonen).

0008-8846/$ - see front matter © 2007 Elsevier Ltd. All rights reserved.
doi:10.1016/j.cemconres.2007.04.004

Table 1
Characteristics of rebar coating materials

Material	Morphology	Average particle size (μm)	Composition (% of total weight)								
Silicon powder	Crystalline	4.13	Si								
			99.99								
Silica Fume	Amorphous	<1	SiO_2	MgO	Al_2O_3	CaO	SO_3	Fe_2O_3	Na_2O	TiO_2	K_2O
			99.9	0.075	0.031						
Slag	Amorphous	7.16	30.9	9.7	6.9	46.7	2.56	1.15	1.07	0.49	0.43
"NiCrB"	Spherical	0–45	Ni	Cr	B	Fe	Si	C			
			82.35	10	2.5	2.5	2.5	0.15			

coating, which enables penetration of chloride, water and oxygen and enhances corrosion. Cathodic protection is relatively expensive, and requires manpower in the setup and maintenance [13–15].

In view of the downsides of both the epoxy coating and cathodic protection, NSF initiated a preliminary research investigation aiming at fabricating a robust double-layer coating that provides better abrasion and impact resistance than epoxy on one hand, and cost competitive to cathodic protection through the service life of the concrete member on the other hand.

The objectives of this study are to evaluate the performance of a new double-layer coating composed of NiCrB and an inorganic layer and evaluate the relative contribution of each layer to the corrosion protection. The working hypothesis was that the performance of the inorganic layer would be enhanced due to pozzolanic reaction.

2. Materials and procedures

2.1. The coating materials and compositions

Crystalline silicon powder, silica fume, and amorphous slag were used as inorganic outer coating layer. Table 1 shows the compositions and particle sizes of these materials. The dowels are coated in two steps: (1) The NiCrB sub-layer is applied using a Metco 5P thermal spray gun at a nominal feed rate of 0.68 kg/h (1.5 lb/h). In this process the particles are melted in an oxygen and acetylene flame at a nominal gas flow of 4.25 m^3/h (150 cf/h). (2) The inorganic coating is applied with an SG-100 plasma gun at about the same nominal rate as the NiCrB. The temperature of the plume (argon/hydrogen mix) at the nozzle tip is approximately 8300 °C, but due to the large quantities of air entrained by the plasma plume, the temperature drops down rapidly and the average temperature at the rebar level 3 inches away from the nozzle is only about 2200 °C [16]. This process takes a few seconds only, thus the mechanical properties of the steel rebar are unaffected by this brief intense heat. It follows that both layers are supposed to provide good protection against corrosion due to the formation of impervious coatings at these high temperatures. Table 2 shows the mixture proportions of the coatings used in this study.

Evidently, this process is energy intensive and costs more than the simple epoxy coating technique. However, provided that a robust coating that extends the service life of the member is formed, on a life cycle basis, the materials cost and fabrication might have a minor effect. In this sense, this technique might turn to be quite effective in suppressing both rate of corrosion and life cycle costs, especially in environments subjected to numerous freeze–thaw cycles and frequent applications of deicers.

Two series (denoted 1 and 2) were produced. The first ("Series 1") is made up of coatings 1–1 through 1–7 as listed in Table 2. In addition, a plain A36 rebar designated as 1–9 was used as a reference. Based on the best performing coating from Series 1, the coating composition in "Series 2" was modified by changing the thickness of NiCrB (7 and 10 mils, i.e., about 180 and 250 μm, respectively) and applying the outer coating at different working conditions: half the nominal powder feedrate and half the nominal gas flow. The pozzolanic activity of each of the inorganic materials was evaluated individually as described in Section 2.3.

Table 2
Coating compositions

Bar #	NiCrB sub-layer	5 μm Silicon powder (%)	Cabosil[a] (%)	Slag (%)	Powder federate	Gas flow
1–1	7 mils	100	0	0	1	1
1–2	7 mils	0	100	0	1	1
1–3	7 mils	10	0	90	1	1
1–4	7 mils	4	6	90	1	1
1–5	7 mils	0	10	90	1	1
1–6	n/a	10	0	90	1	1
1–7	n/a	0	10	90	1	1
2–1	7 mils	n/a	n/a	n/a	n/a	n/a
2–2	10 mils	n/a	n/a	n/a	n/a	n/a
2–3	7 mils	n/a	10	90	1	1
2–4	7 mils	n/a	10	90	1/2	1
2–5	7 mils	n/a	10	90	1	1/2

[a] Silica fume (Cabot Corp.).

2.2. Pore solution: expression and composition

In order to simulate a realistic environment, the dowels were immersed in solutions similar in composition to the solution expressed from Lafarge Type I portland cement of composition given in Table 3.

Pastes prepared at w:c 0.55 according to ASTM Standard C305-82 were placed in a 100 × 200 mm plastic cylinder, immediately sealed off with plastic sheets, and cured at room temperature. The extraction of the pore fluids was performed at 1.5, 2, 4.5, 8, and 24 h. Up to 4.5 h, extractions were done by placing the

Table 3
Oxide and Bogue composition of type I portland cement

Compound	CaO	SiO_2	Al_2O_3	Fe_2O_3	MgO	SO_3
Weight (%)	65.3	20.4	4.8	2.8	2.2	2.5
Bogue	C3S	C2S	C3A	C4AF		
	67.4	7.6	8.0	8.5		

Table 4
Composition of the simulated pore solution, mmol

Ca^{2+}	Na^{+}	K^{+}	SO_4^{2-}	OH^{-}	pH (theoretical)
13.28	104	243	22	316	13.5

pastes in a büchner funnel and filtered through a 0.45 μm filter paper by applying a vacuum via a rotary pump. At later ages, the pore solutions were extracted by placing the pastes in a steel die and exerting a compressive load with a hydraulic press in a similar way as described by Barneyback and Diamond [17].

Immediately after extraction, the solutions were diluted five times with double-distilled water and acidified with hydrochloric acid at 1% g/g ratio. This measure was taken in order to prevent salt precipitation prior to chemical analysis and to minimize dilution errors. A Perkin-Elmer 40 Inductively Coupled Plasma Spectrophotometer was used for determining the elemental concentrations of Na, K, Ca, Si, and Al. The alkalinity of each solution was determined immediately after the extraction by a pH meter. The sulfate content was calculated by difference. Fig. 4 shows the evolution of concentration of the species in the extracted pore solution over time.

A key objective in this research investigation concerns the performance of a pozzolanic material as a protective layer. Consequently, in order to provide an ample supply of calcium for pozzolanic reactions, the concentration of Ca^{2+} in the synthetic pore solution was doubled to 11.06 mmol and subsequently, the ionic strength of the pore solution was further increased by 20% to 0.4. This adjustment, increased the initial concentration of Ca2+ to 13.28 mmol and the pH to 13.5. Oversaturation with respect to calcium was deemed necessary in order to prevent depletion of calcium ions from the synthetic solution in case of pozzolanic reaction. It should also be noted that the ionic strength of pore fluids of most of commercial cements is lower than 0.4. The composition of the synthetic pore solution is given in Table 4.

Analytical grade reagents of calcium hydroxide, sodium and potassium hydroxide, and potassium sulfate were used in the preparation of the simulated pore solution. In view of the low concentrations of silicon and aluminum, these species were excluded from the pore solution. The coated rebars were immersed in two plastic tubs, each containing a total of 15 L of simulated solution.

2.3. Pozzolanic activity of the raw coating materials

The benefits associated with incorporating pozzolanic materials in cementitious materials have been extensively studied [18–21,35]. Most of the literature though, deals with properties, such as microstructure, strength, durability, transport properties, etc. For this application, what matters is whether pozzolanic activity by itself adds value in protecting the steel dowels.

The proportions for the mixes of each of the raw materials with calcium hydroxide were based on the assumption that the calcium/silica ratio of the pozzolanic product will be smaller than Ca/Si=2.0 [22,23]. For the calcium hydroxide/slag mix, a more complex computation was carried out. Since the slag contains appreciable amount of alumina that may react with calcium, a Ca/(Si+Al) =2.0 was chosen. This "hydraulic factor", for simplifying purposes is slightly modified with respect to formulae in another study [21]. Subsequently, based on the chemical composition of each raw material, these atomic ratios were converted into mass ratios.

After mixing with double-distilled water at w:c 0.55, each mixture was placed in 5 glass vials that were then sealed and reopened only when hydration was to be stopped at 3, 7, 14, 28 and 56 days after mixing. Hydration was stopped by grinding the specimen in a mortar with methanol for 20 min and then filtering the slurry with a vacuum pump until a fine, dry powder is obtained. This powder is then placed in a new sealed vial and stored for subsequent analyses.

Reference "dry mixes" were also made for XRD analyses. These mixtures contained no water and therefore served as references for zero hydration. Consequently, their diffraction patterns could be directly compared with those of the hydrated mixes. This simple procedure enabled a direct evaluation of the pozzolanic activity of the materials at a given testing age by comparing the relative height of the calcium hydroxide peaks and noting the appearance of new peaks that indicate formation of new phases.

In addition, in order to quantify the degree of pozzolanic reaction, thermogravimetric analyses (TGA) were also carried out using a Mettler Toledo apparatus from 25° to 1000 °C at 10°/min.

2.4. Corrosion resistance measurements with alternating current impedance spectroscopy

The research investigation was divided into two series denoted as 1 and 2. In each series the identical dowels were immersed in two tanks denoted hereafter as Tank#1 and Tank#2. Both tanks contained the plain pore solution, but the solution in Tank #2 contained also sodium chloride. The sodium chloride at a concentration of 3.5% by mass of the pore solution was added to Tank #2 after 14 days of immersion of the dowels in plain pore solution. In Series 1, the dowels designated as "1–1" thru "1–7" as well as the reference plain steel dowel "1–9" (Table 2) were immersed in both tanks until testing. Testing of the dowels immersed in both tanks was conducted every 7 days up to 28 days and then every 14 days up to 70 days.

Tanks # 1 and #2 were also used to test the dowels designated as "2–1" thru "2–5" in Series 2. Similar to the first series, the dowels in Tank #1 were immersed in pore solution only, whereas 3.5% sodium chloride by mass of the pore solution was added to Tank #2 after the first 14 days of immersion in the plain pore solution. The testing was carried out every 7 days up to 42 days after the initial immersion in the fluids.

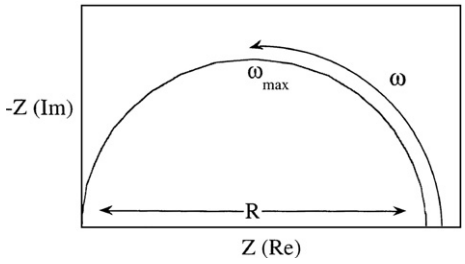

Fig. 1. Theoretical Nyquist plot for simple parallel RC circuit.

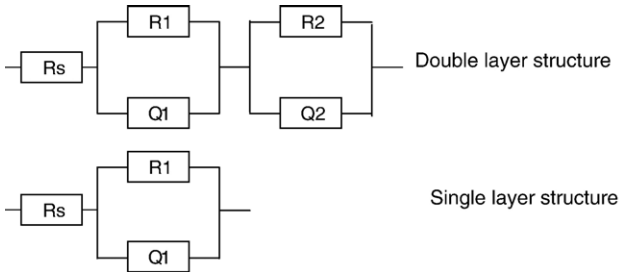

Fig. 2. Equivalent circuits used in the fitting of impedance data.

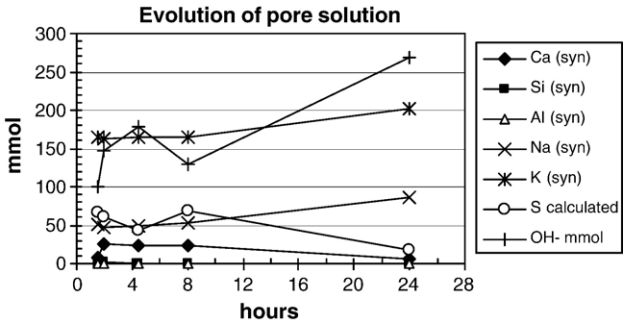

Fig. 4. Evolution of elemental concentrations in expressed Type I portland cement pore solution.

The basic impedance spectroscopy experiment consists of applying an alternating signal (generally, but not limited to, sinusoidal) and measuring the subsequent (current) response of the system. All materials, to varying degrees, pass current, and voltage and current follow Ohm's law for DC fields. In the case of AC fields, the relationships between voltage and current are:

$$V(\mathrm{t}) = I(\mathrm{t})Z(\omega) \tag{1}$$

where V(t) and I(t) are the time-dependant voltage and the current respectively. The quantity $Z(\omega)$ is defined as the frequency-dependent impedance, with ω being the angular frequency of the signal. Typically, this study included, impedance measurements involve the use of pure sine wave signals for the excitation voltage. That results in a current that is also a sine wave of same frequency, but with a phase offset θ:

$$V(\mathrm{t}) = V_0 \sin(\omega \cdot t) \tag{2}$$

$$I(\mathrm{t}) = I_0 \sin(\omega \cdot t + \theta) \tag{3}$$

The frequency-dependent impedance is a complex function, having both real (Z') and imaginary (Z'') components. The most common way of representing the data is the so-called Nyquist plot (Fig. 1) where data is plotted in the (Z', $-Z''$) plane. This plot shows the dual resistive/capacitive behavior of an electrochemical system. The resistive behavior stems from the ability of the electrode (rebar sample) to impede the current flow, whereas the capacitive behavior relates to the ability of the system to "store" electrical charge. From a corrosion standpoint, the "diameter" of the impedance arc (R) is of importance, because in the frequency domain selected for this study, it is directly related to the resistance of the coated dowel.

It should be noted that the value for R can only be obtained by the difference of the measured impedance at sufficiently high and low frequencies, which theoretically is given by [32]:

$$R = |Z(\omega)|_{\omega\text{-}0} - |Z(\omega)|_{\omega\sim\infty} \tag{4}$$

The value of the arc diameter is independent of the type of the equivalent circuit used to model the impedance arc, because Eq. (4) does not include any capacitive component. The corrosion resistance is determined by extrapolating the experimental portion of the arc towards the right of the Nyquist plot (i.e., towards the very low frequency range). To obtain the numerical value of R, equivalent circuit software was used to fit the experimental data [38]. For the sake of simplicity, the circuits in Fig. 2 were used to model single and double-layer coatings. The

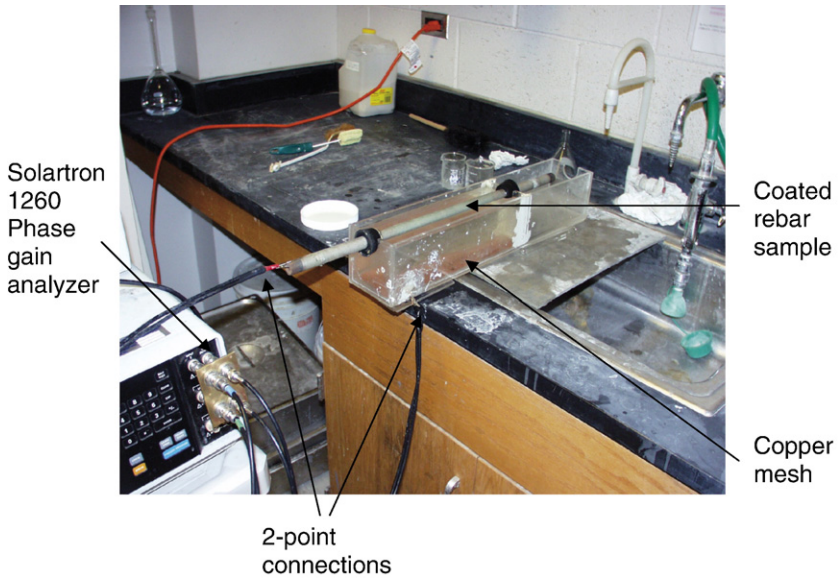

Fig. 3. Experimental setup for AC impedance spectroscopy measurements.

"*Q*" element represents a "constant phase element," CPE, which replaces a pure capacitor component. The CPE term is introduced in order to account for the "depression" below the Z' (real impedance) axis that is frequently observed in non-ideal systems. Further details on the causes of arc depression can be found in the literature [32, 27–29]. Details on the equations related to equivalent circuit modeling are given elsewhere [26,33].

Fig. 3 shows the setup for measuring the corrosion resistance. The coated rebar acts as a working electrode, a copper mesh with high surface area placed below the coated bar acts as a counterelectrode, and the simulated pore solution (that was taken from the same tank that the tested rebar was immersed in) acts as a conducting medium. In this setup, referred to in the literature as "2-point" configuration, the impedance measured is equal to the total impedance of both electrodes and the conductive medium [24,25]. However, due to the high conductivity of the electrolyte, it is unlikely that its contribution to the total impedance is significant. In order to determine the influence of the copper mesh on the impedance results, the coated dowel was replaced by a copper mesh of identical dimensions of that of the counterelectrode, and was placed at the same height as the coated dowel. The resulting impedance plot was insignificantly

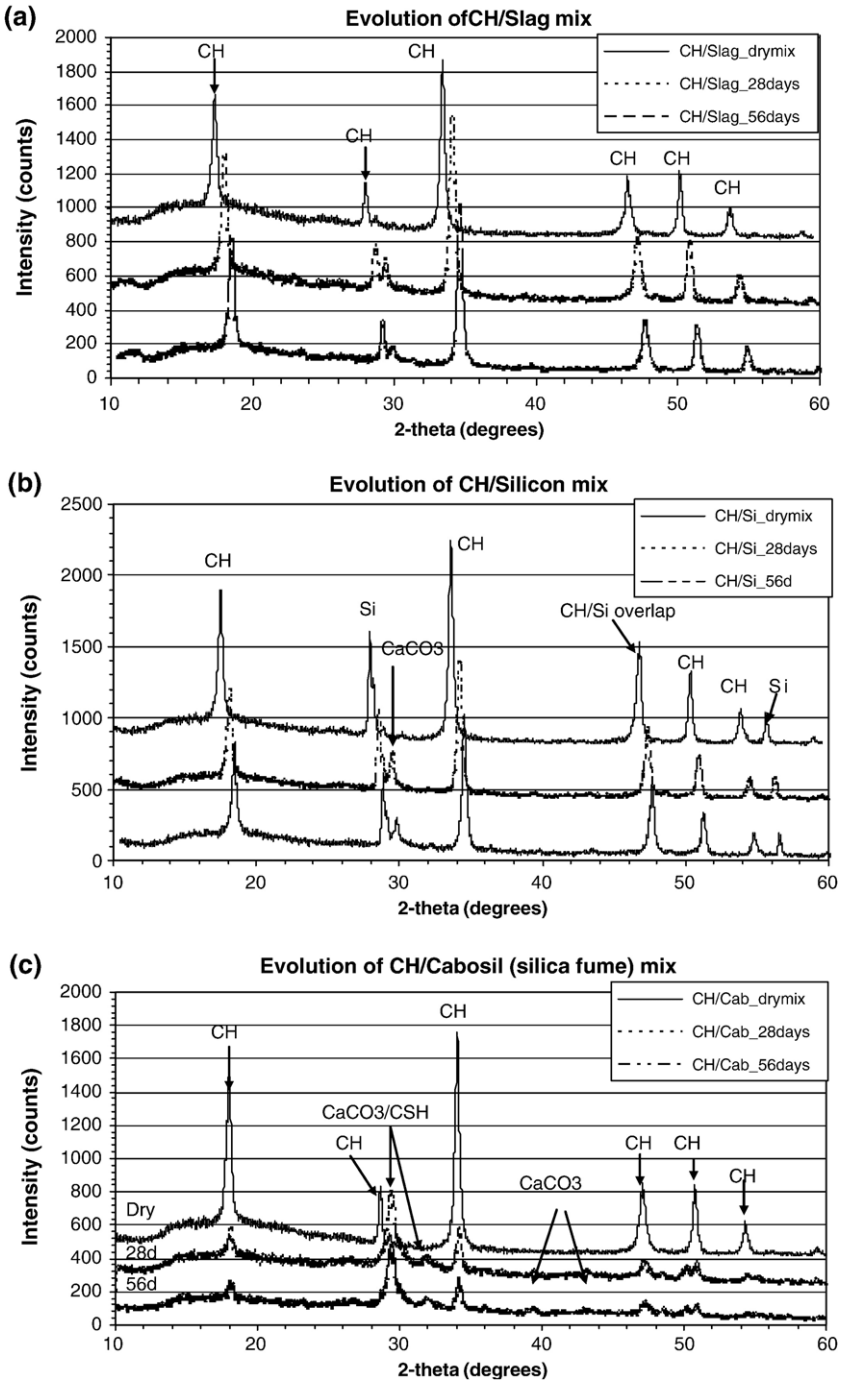

Fig. 5. X-Ray diffractograms of hydrated calcium hydroxide-slag (a); -silicon powder (b); -silica fume (c) mixes.

Table 5
Results from thermogravimetric analyses

Mix type	% initial CH in dry mix	% CH in hydrated	% $CaCO_3$
CH/Cab 3 days	71.3	6.6	5.2
CH/Cab 7 days	71.2	4.7	3.2
CH/Cab 14 days	71.2	5.7	1.9
CH/Cab 28 days	70.8	4.0	6.0
CH/Cab 56 days	71.4	4.0	7.9
CH/Slag 14 days	69.5	44.5	5.5
CH/Slag 28 days	69.6	43.8	7.7
CH/Slag 56 days	69.6	43.2	5.4
CH/Si 14 days	84	39.2	6.6
CH/Si 28 days	84.1	35.9	8.1
CH/Si 56 days	84	35.6	5.7
CH only	n/a	91.5	5.2

small compared to results obtained with the dowels, with an arc amplitude up to 1000 times smaller.

Following some preliminary tests, all the measurements were carried out at a frequency range of 10 mHz to 10 kHz, voltage amplitude of 25 mV, and 50 or 60 scanned points. This frequency domain is in agreement with literature related to the impedance response of cement-based systems as well as systems involving a purely liquid electrolyte [26–31]. The voltage amplitude is kept sufficiently low, thus avoiding stability problems, especially in the lowermost portion of the scanned frequency range.

3. Results and discussion

3.1. Pore solution composition

Fig. 4 shows the evolution of the elemental concentrations. Accordingly, the concentrations of OH^-, K^+, and Na^+ continuously increase; the content of S^{6-} moderately increases during the first 8 h and then is continuously depleted. In contrast, the solubility of Ca^{2+}, Al^{3+}, and Si^{4+} is much smaller, and apart from the first 2 h, these cations are continuously removed from the pore solution. Therefore, at 24 h, the concentrations in the expressed pore fluid of OH^-, K^+, Na^+, S^{6-}, Ca^{2+}, Si^{4+}, and Al^{3+} are about 269, 202, 87, 17.3, 5.53, 0.55, and 0.44 mmol, respectively. Table 4 shows the final composition of the simulated pore solution after corrections as mentioned in Section 2.2.

3.2. Measurement of pozzolanic activity

The X-Ray diffractograms (Fig. 5a–c) show the major peak heights of the hydrated samples at 28 and 56 days after hydration along with the diffractogram of the "dry mix" (calcium hydroxide+coating materials without water).

As a preliminary conclusion, it appears that the slag (Fig. 5a) exhibits a rather sluggish reaction with calcium hydroxide (CH) as hardly any decrease in the CH peak height is observed between the reference dry mix (0 hydration) and 28 days of hydration. At a longer period between 28 and 56 days only a very slight decrease is visible.

In the case of the silicon mixes (Fig. 5b), somewhat more rapid reaction seems to have taken place, which is detected by the decrease of the intensities of the CH peaks between 0 and 28 days and a smaller decrease from 28 to 56 days. The sharper $CaCO_3$ peak appearing at both 28 and 56 days was attributed to carbonation already present in the $Ca(OH)_2$ reagent, and further carbonation during preparation and curing.

The greatest uptake of $Ca(OH)_2$ is viewed in the CH/silica fume mixes (Fig. 5c), where a drastic decrease in the CH peak heights is observed between 0 and 28 days followed by a much

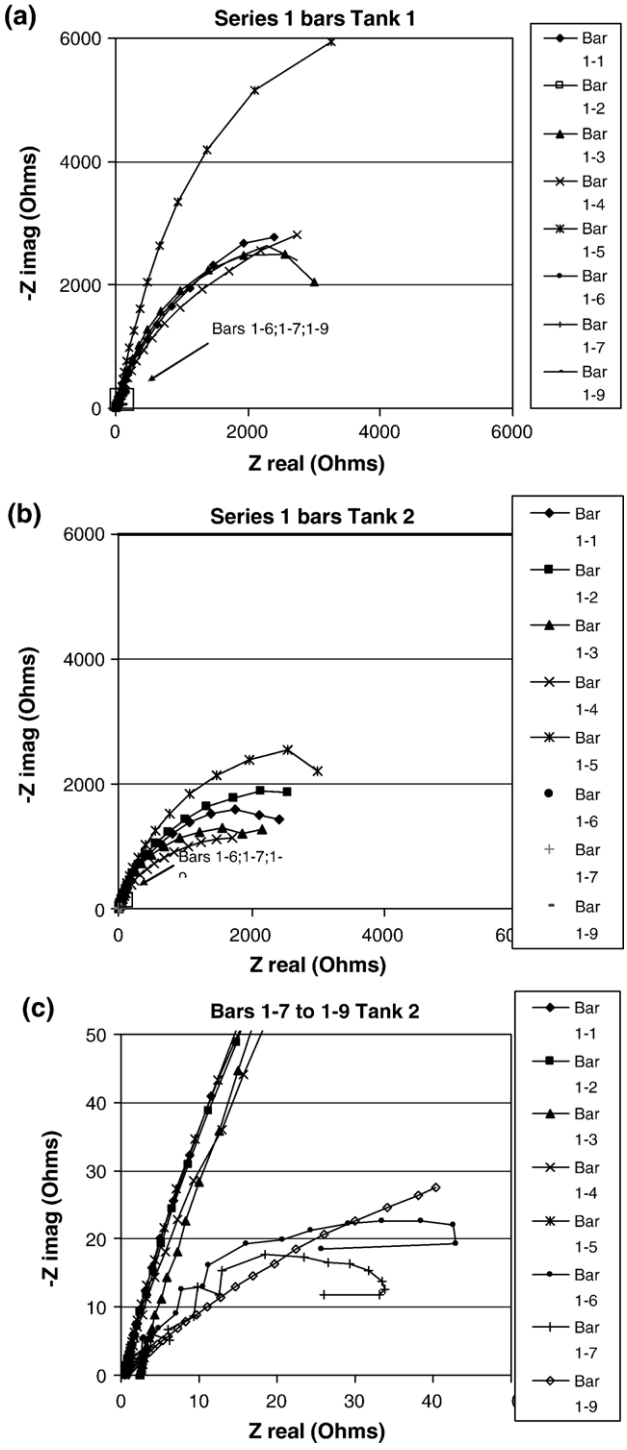

Fig. 6. (a) Nyquist plots for Series 1 dowels in Tank #1 at 70 days. (b) Nyquist plots for Series 1 dowels in Tank #2 at 70 days. (c) Close-up on bars 1–6 to 1–9, Tank #2.

Table 6
Values of corrosion resistance (R_p) as obtained by data-fitting (Ω)

Bar #	1–1	1–2	1–3	1–4	1–5	1–6	1–7
Tank1	7735	7327	6117	7114	27854	875	964
Tank2	4046	4771	3125	2865	6516	59.7	42.8

smaller one between 28 and 56 days of hydration. This marked consumption of CH is associated with the appearance of C–S–H [34].

The distinct appearance of $CaCO_3$ in all the diffractograms was puzzling. Therefore, a sample of the $Ca(OH)_2$ reagent used in the mix preparations was analyzed by XRD and a small amount of calcite was detected. TGA analysis confirmed a presence of about 5.2% calcite.

Table 5 summarizes the thermogravimetric results. The table data represents the percentage by weight of CH present in each of the mixes. The leftmost column of data represents the percentage of CH in the dry mixes (prepared without water) that served as a reference to compare hydrated mixes at given points in time. The initial quantity of calcium carbonate present when the paste preparation took place is variable. The CH/Si mixes were the first to be prepared and hence were likely to have the higher average carbonate content (6.8%). On the other hand, the silica fume based mixes were the last in the preparation sequence and have overall a lower average carbonate content of 4.8%. Given the experimental protocol utilized, it seems that only minimal if any additional carbonation would have taken place during the curing of the samples. Consequently, the amount of calcite detected by TGA is probably very similar to the amount initially present when the mixes were prepared.

In agreement with the XRD results, Table 5 shows that the highest consumption of CH takes place in the silica fume mixes. In fact, the preponderant amount of CH is consumed in the first three days of hydration and less than 3% of CH is further consumed between 3 and 8 days. The CH consumption rates of silicon and slag mixtures are by far lower than that of the silica fume, and that of silicon mixtures is greater than that the corresponding slag mixtures. These results are somewhat

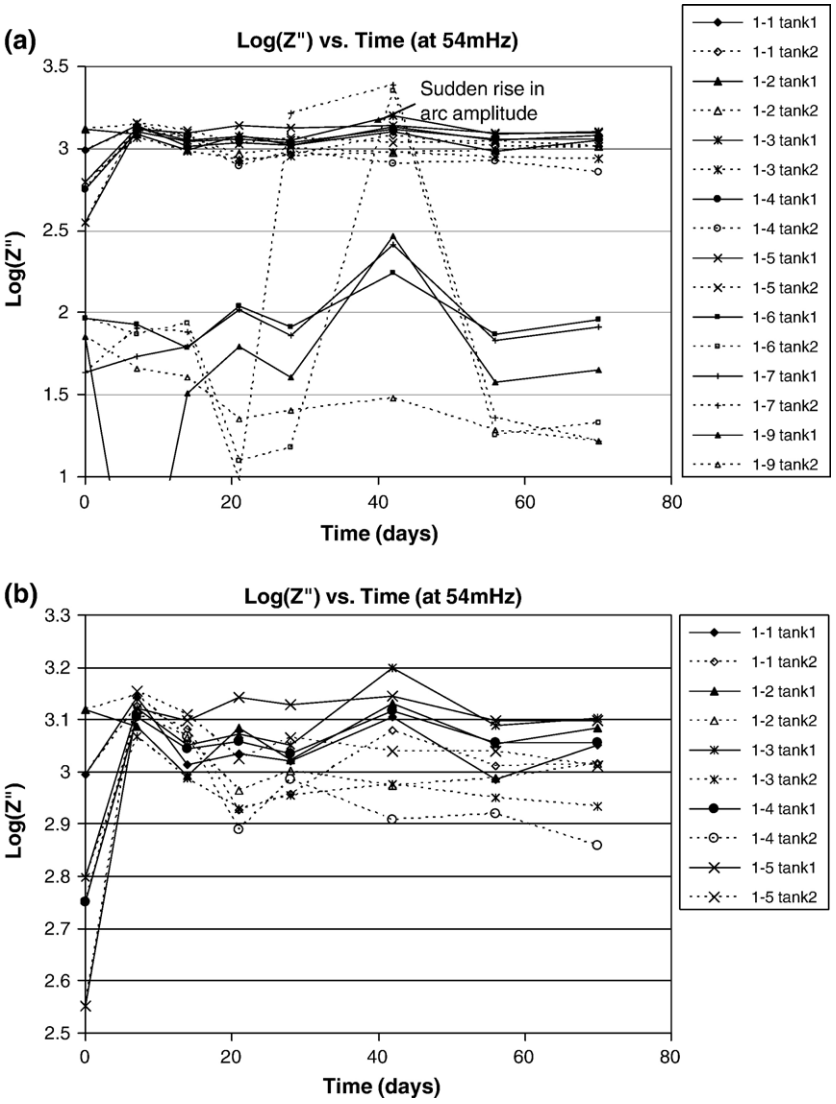

Fig. 7. Logarithmic plots of imaginary impedance (Z") vs. time at 54 mHz for Series 1 (a); for bars 1–1 to 1–5 (b).

atypical given the crystalline nature of the silicon powder as opposed to the rather amorphous state of the slag. The higher reactivity of silicon may be attributed in part to the difference in the average particle size of these substances being 4.13 μm for the silicon powder and 7.6 μm for the slag. Nonetheless, this modest difference in size cannot provide a satisfactory explanation, but concluding that this slag has a low rate of pozzolanic reactivity.

3.3. The resistance of Series 1 dowels to corrosion

The resistance to corrosion can be evaluated from the shape of the Nyquist plots. A good resistance is provided if a steep "incipient" arc is obtained. The steeper the incipient arc is, the larger the extrapolated semi-circle will be, hence a larger value for the arc diameter read on the real impedance (Z') axis.

Due to the large amount of data collected, Fig. 6a shows only the Nyquist plots of the different coatings immersed for 70 days in the plain synthetic pore solution (Tank #1), whereas Fig. 6b,c show the corresponding plots the dowels immersed in the pore solution with 3.5% sodium chloride (Tank #2). Table 6 provides the numerical values of R_p as determined from the equivalent circuit software. In accordance with the criterion given above, Fig. 6 and Table 6 show that bar 1–5 with the inner NiCrB layer and an outer layer of 10% silica fume+90% slag exhibits the best overall performance up to 70 days exposure to simulated pore solution (56 days exposure to chlorides in Tank # 2).

The working hypothesis was that pozzolanic reaction would densify the inorganic coating that in turn, would increase the resistance to corrosion. It had been shown that silica fume had the highest rate of pozzolanic reaction, whereas slag the lowest one. Nonetheless, the outer coating of rebar 1–5 made with 90% slag and only 10% silica fume provides a better resistance than rebar 1–2 (100% silica fume outer layer). It is interpreted therefore, that particle packing decreases the rate of diffusion of the solution within the coating and is more important that any modification of the structure due to pozzolanic activity. Indeed subsequent SEM micrographs show that the slag–silica fume coating is more compact than that of the silica fume layer.

Another way of highlighting the enhanced performance of the NiCrB-coated specimens is to plot the logarithm of the imaginary impedance at a fixed frequency versus time. Fig. 7a and b were plotted at a fixed frequency value of 54 mHz, i.e. in the electrode (or low frequency arc) range. Even within the "cluster" of bars 1–1 to 1–5 (Fig. 7b), differentiation between best and worse performing coatings can be made although they have to be confirmed from the data collected after equivalent circuit fitting.

In Fig. 7a there is a sudden increase in the value of log(Z'') at 28 and 42 days for bars 1–6 and 1–7, which are made without the NiCrB sub-layer. However, subsequent measurements show a return to values within the range initially observed from 0 to 21 days. Visual observations on these dowels during testing at 28 and 42 days indicated extensive pit formation with large efflorescence of rust products growing out of the pits.

It is believed that these spikes could be caused by some clogging of the pits, which would have produced high-resistance

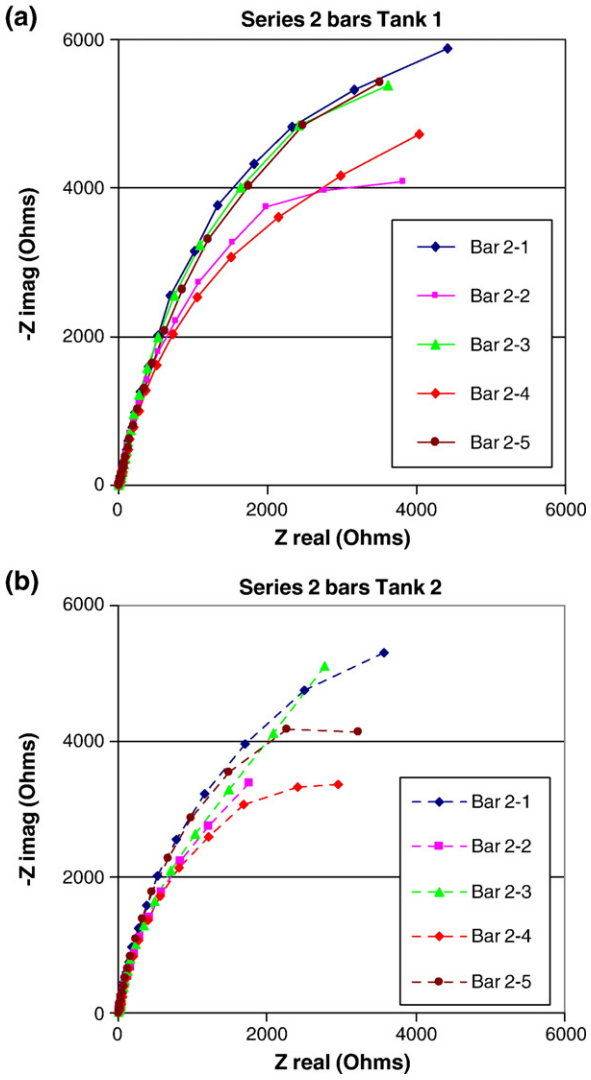

Fig. 8. Nyquist plots of Series 2 dowels at 42 days. Tank 1 (a); Tank 2 (b).

points all along the rebar, hence contributing to the overall response [35]. However, as more rust is generated and the clogging is removed either because of the new volume of rust generated or gravity, active corrosion prevails as reflected by the final data collected at 70 days. Alternatively, a renewed active corrosion can take place as a result of the formation of numerous new pits, thus "overshadowing" the resistance provided by the remaining clogged pits.

It is nevertheless clear from the performance study of the Series 1 dowels that the NiCrB sub-layer is fundamental in providing enhanced corrosion resistance when comparing for example bars 1–5 (NiCrB+10% silica fume+90% slag) and 1–7 (same outer layer as 1–5 with no NiCrB). Dowel 1–7 is an example of an actively corroding surface. This is reflected in the distorted impedance data seen in Fig. 6c [32,36,37]. Indeed active corrosion has been reported to cause distortion in the shape of the Nyquist plots gathered through impedance spectroscopy measurements. The overall diameter of the arc (read on the Real impedance axis) is much smaller than that of a passive highly resistive system.

3.4. Series 2 results

The results from Series 2 are presented in Fig. 8a and b at 42 days for both tanks. The results are consistent with those of Series 1 in the sense that they confirm once again the role of the NiCrB coating in providing overall corrosion resistance. It appears from the Nyquist plot of samples in Tank 1, that bars 2–1, 2–3 and 2–5 have very similar performances when comparing the amplitude of their arcs, which makes it difficult to "rank" them properly. Bar 2–4 (half the powder feedrate) appears consistently below all the other bars in both tanks. It is worth mentioning that no signs of corrosion were reported on any of the ten Series 2 samples tested during the entire duration of the testing program (42 days). In the Nyquist plots bars 2–1, 2–3 and 2–5 have similar performances in Tank #1 but all samples are easily separable in Tank #2. Coating 2–3 has the third best overall performance in Tank #1 and it seems as if this coating performs just as well as a single layer structure (2–1) in Tank #2.

This could put into question the efficiency of the outer layer in providing additional corrosion protection to that provided already by the sub-layer. Also, extensive flaking of this outer layer took place when solution was poured over the rebar while filling the testing tank. The mechanical deterioration of the outer layer was nevertheless not observed while the bars were in the storage tanks.

It should be noted that Series 2 was produced on an exploratory basis, thus changes in the working parameters during the application of the coating could have produced inhomogeneous coating or other flaws that affected the resistance to corrosion. In this regard no direct comparison between Series 1 and 2 results has to be established. This might also explain why the thicker NiCrB layer (2–2) has a lesser performance than the thinner NiCrB layer (2–1).

By changing the working conditions, Fig. 8a shows that the resistance dowel 2–4 is less than 2–3 and 2–5, whereas the resistance of 2–5 and 2–3 is about the same. One explanation to this observation is that the decrease of the gas flow (2–5) increases the temperature, thus a more glassy and uniform coating is formed. In turn, a decrease of the powder federate (2–4) produces a more porous structure [16] that adversely affects the resistance to corrosion.

4. Conclusions

This study shows the useful application of AC Impedance Spectroscopy technique to detect corrosion processes taking place at the surface of a number of coated dowels immersed in simulated pore solution with and without a high concentration of chlorides. The study on Series 1 dowels showed that the NiCrB sub-layer outperforms any of the inorganic coatings and is essential in providing corrosion resistance. Series 2 results confirm the previous results and also illustrate that the properties of the inorganic coating depend on the working conditions.

The external inorganic coating might provide abrasion resistance. However, the working hypothesis that pozzolanic reaction would densify the inorganic coating and increase the resistance to corrosion has been proven as incorrect. Of the inorganic materials used, silica fume has the highest rate of pozzolanic reactivity, whereas the slag has the sluggish one. Nonetheless, the coating comprising 90% slag and 10% silica fume performs better than coating made with silica fume. It implies that particle packing is more important than any changes to the structure of the coating due to pozzolanic reaction.

References

[1] J.P. Broomfield, Corrosion of Steel in Concrete, Understanding, Investigation and Repair, E and FN Spon, 1997.
[2] Federal Highway Administration, Highway Bridge Replacement and Rehabilitation Program (HBRRP) 2002 data (online source), www.fhwa.dot.gov/bridge/transfer.
[3] A. Neville, Chloride attack of reinforced concrete: an overview, Materials and Structures 28 (1995) 63–70.
[4] FIP, Recommendations for the Design and Construction of Concrete Sea Structures, 2nd edition, 1974, pp. 28–30.
[5] P.S. Mangat, B.T. Molloy, Factors influencing chloride-induced corrosion of reinforcement in concrete, Materials and Structures 25 (1992) 404–411.
[6] D.A. Hausmann, Steel corrosion in concrete, Materials Protection 6 (11) (1967) 19–22.
[7] V.K. Gouda, Corrosion and corrosion inhibition of reinforcing steel, British Corrosion Journal 5 (9) (1970) 198–203.
[8] Guide to durable concrete, Chapter IV—Corrosion of Steel and Other Materials, Manual of Concrete Practice Part 1, vol. 201, ACI Committee, 1994.
[9] C. Alonso, C. Andrade, M. Castellote, P. Castro, Chloride threshold values to depassivate reinforcing bars embedded in standardized OPC mortar, Cement and Concrete Research 30 (2000) 1047–1055.
[10] C.L. Page, P. Lambert, P.R.W. Vassie, Investigations of reinforcement corrosion, Part 1: the pore electrolyte phase in chloride contaminated concrete, Materials and Structures 24 (1991) 243–252.
[11] P. Lambert, C.L. Page, P.R.W. Vassie, Investigations of reinforcement corrosion, Part 2: electrochemical monitoring of steel in chloride-contaminated concrete, Materials and Structures 24 (1991) 351–358.
[12] D.G. Manning, Corrosion performance of epoxy-coated reinforcement steel: the North American experience, Construction and Building Materials 10 (5) (1996) 349–365.
[13] B.S. Covino Jr., S.D. Cramer, G.R. Holcomb, S.J. Bullard, G.E. McGill, C. B. Cryer, Thermal-sprayed Zinc anodes for cathodic protection of reinforced concrete structures, in: Ken P. Chong (Ed.), Materials for a New Millenium, 1997.
[14] J. Christopher Ball, David W. Whitmore, Corrosion mitigation systems for concrete structures, Concrete Repair Bulletin (July/August 2003) 6–11.
[15] Bertolini, et al., Cathodic protection and cathodic prevention in concrete; principles and applications, Journal of Applied Electrochemistry 28 (1998) 1321–1331.
[16] Dominic J. Varacalle, Jr., Director of Vartech Inc., Idaho Falls ID Personal communication.
[17] R.S. Barneyback, S. Diamond, Expression and analysis of pore fluids from hardened cement pastes and mortars, Cement and Concrete Research 11 (1981) 279–285.
[18] A.S. Al-Ghatani, S.S. Rasheeduzzafar, Al-Saadoun, Rebar corrosion and sulfate resistance of blast furnace slag cement, Journal of Materials in Civil Engineering 6 (3) (1993) 223–239.
[19] D.P. Bentz, P.E. Stutzman, Evolution of porosity and calcium hydroxide in laboratory concrete containing silica fume, Cement and Concrete Research 24 (6) (1994) 1044–1050.
[20] W. Eitel, Ceramics and hydraulic binders, Silicate Science, vol. 5, Academic Press, 1966.
[21] Sujin Song, Hydration of ground granulated blast furnace slag, PhD Dissertation, Northwestern University, 1998.
[22] D. Rothstein, J.J. Thomas, B.J. Christensen, H.M. Jennings, Solubility behavior of Ca-, S-, Al- and Si- bearing solid phases in Portland cement pore

solutions as a function of hydration time, Cement and Concrete Research 32 (2002) 1663–1671.
[23] Paul W. Brown, The system Na_2O–CaO–SiO_2–H_2O, Journal of the American Ceramic Society 73 (11) (1990) 3457–3461.
[24] G. Hsieh, Applications of impedance spectroscopy to the characterization of solid electrolyte material systems, PhD Dissertation, Northwestern University.
[25] T.O. Mason, S.J. Ford, J.D. Shane, J.-H. Hwang, D.D. Edwards, Experimental limitations in impedance spectroscopy of cement-based materials, Advances in Cement Research 10 (4) (1998) 143–150.
[26] Steven J. Ford, Monitoring the corrosion of reinforcing steel in cement-based systems using impedance spectroscopy, PhD Dissertation, Northwestern University, 1998.
[27] Bruce J. Christensen, Microstructure studies of hydrating portland cement-based materials using impedance spectroscopy, PhD Dissertation, Northwestern University, 1993.
[28] T.O. Mason, Steven J. Ford, Monitoring the corrosion of reinforcing steel in cement-based systems using impedance spectroscopy, in: K.L. Scrivener, J.F. Young (Eds.), Mechanisms of Chemical Degradation of Cement-based Systems, E&FN Spon, 1997.
[29] B.J. Christensen, R. Tate Coverdale, R.A. Olson, S.J. Ford, E.J. Garboczi, H.M. Jennings, T.O. Mason, Impedance spectroscopy of hydrating cement-based materials: measurement, interpretation and application, Journal of the American Ceramic Society 77 (11) (1994) 2789–2804.
[30] Brian B. Hope, Alan K. Ip, Corrosion and electrical impedance in concrete, Cement and Concrete Research 15 (1985) 525–534.
[31] W.J. McCarter, S. Garvin, N. Bouzid, Impedance Measurements on Cement Paste, Chapman and Hall, 1988, p. 1057–1057.
[32] J. Ross Macdonald, Impedance Spectroscopy: Emphasizing Solid Materials and Systems, John Wiley and Sons, 1987.
[33] D. Jolivet, Corrosion resistance of functionally graded coatings on steel reinforcement Bars, MSc Thesis, Northwestern University, 2004.
[34] F. Rendell, R. Jauberthie, M. Grantham, Deteriorated concrete: inspection and physiochemical analysis, Thomas Telford, London, 2002.
[35] T.O. Mason, Personal communication, Oct. 2003.
[36] Ping Gu, Ping Xie, J.J. Beaudouin, Characterization of surface corrosion of reinforcing steel in cement paste by low frequency impedance spectroscopy, Cement and Concrete Research 24 (2) (1994) 231–242.
[37] D.F. Wei, I. Chatterjee, D.A. Jones, Evaluation of corrosive degradation in coated steel using alternating current impedance spectroscopy, Corrosion Science 51 (2) (1995) 97–104.
[38] B.A. Boukamp, Equivalent Circuit (EQUIVCRT.PAS), University of Twente, Netherlands, 1988.